

Modelling the mass-metallicity relation of star-forming galaxies from $z \sim 3.5$ to $z \sim 0$

Jianhui Lian^{*}, Daniel Thomas, Claudia Maraston

Institute of Cosmology and Gravitation, University of Portsmouth, Burnaby Road, Portsmouth, PO1 3FX, UK

10 March 2024

ABSTRACT

We study the origin and cosmic evolution of the mass-metallicity relation (MZR) in star-forming galaxies based on a full, numerical chemical evolution model. The model was designed to match the local MZRs for both gas and stars simultaneously. This is achieved by invoking a time-dependent metal enrichment process which assumes either a time-dependent metal outflow with larger metal loading factors in galactic winds at early times, or a time-dependent Initial Mass Function (IMF) with steeper slopes at early times. We compare the predictions from this model with data sets covering redshifts $0 \leq z \leq 3.5$. The data suggests a two-phase evolution with a transition point around $z \sim 1.5$. Before that epoch the MZR_{gas} has been evolving parallel with no evolution in the slope. After $z \sim 1.5$ the MZR_{gas} started flattening until today. We show that the predictions of both the variable metal outflow and the variable IMF model match these observations very well. Our model also reproduces the evolution of the main sequence, hence the correlation between galaxy mass and star formation rate. We also compare the predicted redshift evolution of the MZR_{star} with data from the literature. As the latter mostly contains data of massive, quenched early-type galaxies, stellar metallicities at high redshifts tend to be higher in the data than predicted by our model. Data of stellar metallicities of lower-mass ($< 10^{11} M_{\odot}$), star-forming galaxies at high redshift is required to test our model.

Key words: galaxies: evolution – galaxies: fundamental parameters – galaxies: star formation.

1 INTRODUCTION

Metallicity, defined as the fractional abundance of elements heavier than Helium, is a key parameter in galaxy evolution models, playing an important role in a number of fundamental astrophysical processes such as star formation, gas cooling, and dust formation. A tight correlation between the metallicity of ionized gas and stellar mass of star forming galaxies has been found for decades (Lequeux et al. 1979). This mass-gas metallicity relation (hereafter MZR_{gas}) was later confirmed to be valid over three orders of magnitude in galaxy stellar mass through the analysis of large galaxy samples from the Sloan Digital Sky Survey (SDSS, York et al. 2000) using various gas metallicity calibrations (Tremonti et al. 2004; Kewley & Ellison 2008; Andrews & Martini 2013). More recently, the MZR_{gas} was detected down to the very low mass end ($M_{\star} < 10^9 M_{\odot}$, Henry et al. 2013a,b; Lian et al. 2016). Furthermore, based on deep spectroscopy of distant galaxies, several studies found that the relation was already well established at high redshift since at least $z \sim 3.5$

(Savaglio et al. 2005; Erb et al. 2006; Maiolino et al. 2008; Yabe et al. 2014; Ly et al. 2016; Kashino et al. 2017). Compared to local star forming galaxies, high redshift objects at the same stellar mass are generally found to be more metal poor in the ionized gas by ~ 0.3 dex at $z \sim 2$ (Erb et al. 2006).

However, the exact evolution of the MZR_{gas} with time and the physical drivers of such evolution is a matter of debate. Using the ‘Te’ method to derive gas metallicity, Ly et al. (2016) find no clear evolution in the slope of the MZR_{gas} since $z \sim 1$. Kashino et al. (2017), instead, in a study based on large galaxy samples from the FMOS-COSMOS survey find the MZR_{gas} to be significantly steeper at $z \sim 1.6$ than at $z = 0$. Interestingly, a flattening of the MZR_{gas} relation with cosmic time is consistent with prediction from cosmological hydrodynamical simulations (Guo et al. 2016; Taylor & Kobayashi 2016).

Further constraints on the metal enrichment history of galaxies and hence the evolution of the MZR_{gas} can be obtained from the local mass-*stellar* metallicity relation (hereafter MZR_{star}), since the stellar metallicity carries information on the past metal enrichment. In Lian et al. (2018)

^{*} jianhui.lian@port.ac.uk

(hereafter Paper I) we simultaneously analyse the MZR_{gas} and MZR_{star} of local star forming galaxies based on SDSS data and a full, numerical chemical evolution model. Because of the relatively low stellar metallicity of the lower-mass galaxies, we find that these relations can be reproduced simultaneously only if a time-dependent metal enrichment process is invoked where the metal-enrichment in low-mass galaxies is suppressed at early times. We showed that such a process could be either metal outflow with higher outflow fractions (i.e. larger metal loading factors) at early times or an IMF with steeper IMF slopes at early times. The former regulates the *metal retention* in galaxies so that more metals are lost at early times, while the latter regulates the *metal production* so that less metals are produced at early times.

In both scenarios, the cosmic evolution of the MZR_{gas} is mostly driven by the efficiency of star formation in galaxies but further regulated by the cosmic evolution of either the metal outflow loading factor or the IMF slope. The aim of the present paper is to test these predictions for the redshift evolution of the MZR_{gas} using observational results at various redshifts up to $z \sim 3.5$.

Throughout this paper, we adopt a standard cosmology with parameters with $H_0 = 71 \text{ km s}^{-1} \text{ Mpc}^{-1}$, $\Omega_\Lambda = 0.73$ and $\Omega_m = 0.27$ (Spergel et al. 2003).

2 OBSERVATIONS

Following Paper I, we select a local sample of star forming galaxies from the SDSS Data Release 12¹ (DR12; Alam et al. 2015) using the following selection criteria: (1) high specific star formation rates, $\log(\text{sSFR}) > -0.6 \cdot \log(M_*/M_\odot) - 4.9$; (2) a stellar mass cut at $M_* > 10^9 M_\odot$; (3) a redshift range of $0.02 \leq z \leq 0.05$ to ensure mass completeness up to $10^{11} M_\odot$; (4) a high signal-noise-ratio (SNR) above 5 in the strong emission lines (including $\text{H}\beta$, $[\text{O III}]\lambda\lambda 4959, 5007$, $\text{H}\alpha$, $[\text{N II}]\lambda 6584$); (5) a classification outside the composite or AGN region through the demarcation of Kewley et al. (2001) in the BPT diagram (Baldwin, Phillips & Terlevich 1981). The final sample contains 4633 galaxies. Emission line fluxes are corrected for galactic internal extinction using the Balmer decrement method and the Milky Way extinction law (Cardelli et al. 1989). We obtain the gas metallicities of these galaxies using the empirical linear N2 method from Pettini & Pagel (2004), which is widely-used for determining gas metallicities, especially for high-redshift galaxies.

2.1 The mass-gas metallicity relation

Figure 1 shows the local MZR_{gas} we obtain (red line) compared to the same relation at different redshifts as obtained from various works in the literature (other coloured lines as labelled on the plot). In order to enable a proper comparison, stellar masses are corrected to a stellar mass based on the Kroupa IMF and gas metallicities are re-calibrated to the empirical N2 method using the conversion by Maiolino et al. (2008). We adopt a factor of 0.85 to convert the stellar mass based on Salpeter IMF to that based on Kroupa IMF (Maiolino et al. 2008; Bolzonella, et al. 2010; Pforr,

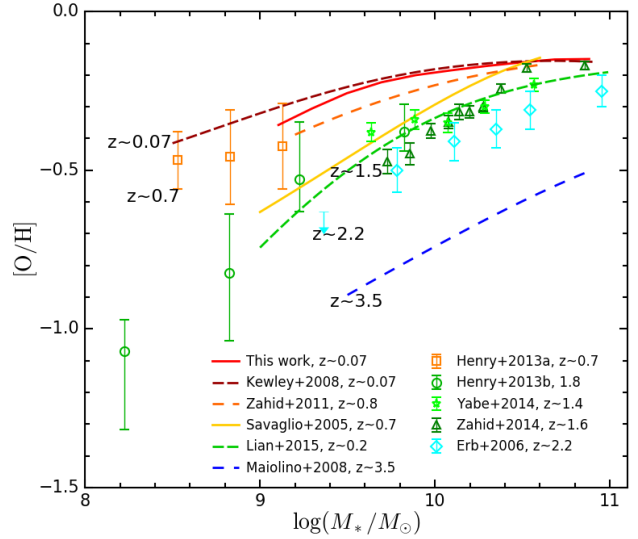


Figure 1. Relation between galaxy stellar mass and gas metallicity at various redshifts. The red solid line is the mass-gas metallicity relation MZR_{gas} at $z \sim 0.03$ as derived in this work. The error bars indicate the 1σ uncertainty of the metallicity measurements. Gas metallicities are re-calibrated to the empirical N2 method (Pettini & Pagel 2004) and stellar masses are corrected to a mass based on a Kroupa IMF.

Maraston & Tonini 2012) and a factor of 1.06 from Chabrier IMF to Kroupa IMF (Mannucci et al. 2010). The typical 1σ uncertainty in gas metallicity in these relations is around 0.1 – 0.2 dex. The MZR_{gas} of a local compact galaxy population named Lyman-break analogues (LBAs), which resemble the relation at $z \sim 1.5$ (Lian et al. 2015), is also included for comparison.

It can be seen that the MZR_{gas} at high redshift is generally steeper than the local one. Most of the evolution of the zero-point of the MZR_{gas} seems to have happened at early times between $z \sim 3.5$ and $z \sim 1.5$ with a significant increase in gas metallicity roughly independent of galaxy stellar mass leaving the slope of the relation unchanged. Subsequently since $z \sim 1.5$ the gas metallicity of the most massive star forming galaxies has not been evolving any further, while most of the evolution is now happening in the lowest mass galaxies. The result is a considerable flattening of the relation between redshift $z \sim 1.5$ and $z = 0$. This mass-dependent gas metallicity evolution has been already noted by Lian et al. (2015) and Kashino et al. (2017) but the physical explanation remains yet to be identified. The invariant gas metallicity in massive galaxies from $z \sim 1.5$ to $z \sim 0$ suggests that these galaxies are already efficiently enriched and their gas metallicity nearly saturates since $z \sim 1.5$, while low-mass galaxies keep evolving in line with the widely accepted picture of downsizing in galaxy evolution

2.2 Comparison with stellar metallicities

In Paper I we derived stellar metallicity from SDSS galaxy spectra using the full spectral fitting code FIREFLY (Wilkinson et al. 2015, 2017) and the stellar population models of Maraston and Strömbäck (Maraston & Strömbäck 2011) (with a Kroupa IMF). The measurement of stellar

¹ <http://www.sdss.org/dr12/>

metallicity is challenging owing to the well-known degeneracy between stellar age, stellar metallicity, and dust extinction (Worthey 1994). Therefore we provide a direct comparison of our results with metallicity measurements from the literature in Paper I. We show that the $\text{MZR}_{\text{stars}}$ used here is in good agreement with the relation in Peng et al. (2015) based on measurements by Gallazzi et al. (2005) and other determinations in the literature (Gallazzi et al. 2005; Panter et al. 2008; Thomas et al. 2010; Johansson et al. 2012). Also, the finding that the $\text{MZR}_{\text{stars}}$ is steeper than the MZR_{gas} (see below) is well in line with the study by González Delgado et al. (2014) where the authors show that average stellar metallicities are generally lower than gas metallicities while the metallicities of the younger populations are higher and match the gas metallicity.

Through the direct comparison between the gas and the stellar metallicities we then constrained the chemical evolution of our galaxy sample. We found that the MZR_{star} is much steeper than the MZR_{gas} , implying a steeper MZR_{gas} at high redshift. This is qualitatively consistent with the finding of a steeper MZR_{gas} at high redshift as shown in Figure 1. We note that Ly et al. (2016) conclude not to find strong evidence for an evolution of the slope of MZR_{gas} since $z \sim 1$, which is at odds with other literature data shown in Figure 1. However, Ly et al. (2016) focus on very low-mass galaxies with masses below $10^9 M_{\odot}$, hence their data does not probe the mass-range within which evolution of the slope appears to occur. To understand the underlying physical processes that drive the evolution of the mass-metallicity relation, a detailed chemical evolution model is required that takes these processes into account.

3 THE CHEMICAL EVOLUTION MODEL

To investigate the physical processes that drive the redshift evolution of the MZR_{gas} , a full chemical evolution model is needed. In Paper I, we develop a numerical chemical evolution model and successfully design it to *simultaneously* reproduce both the MZR_{gas} and the MZR_{star} of local star-forming galaxies.

3.1 Model parameters

The model accounts for three basic physical processes that regulate the chemical evolution of galaxies, namely gas inflow, gas outflow and star formation. We assume a single gas inflow phase whose rate declines exponentially with time. The outflow is characterized by the mass fraction of stellar ejecta that are expelled from the galaxy which is proportional to the mass loading factor defined in the literature as the ratio between the mass of the outgoing baryons and the star formation rate (Veilleux et al. 2005). The empirically-derived Kennicutt-Schmidt (KS, Kennicutt 1998) law is used to set the SFR at a given gas mass (surface density). In total, there are seven basic parameters in the model:

- The coefficient and exponent of the adopted KS law, A_{ks} (normalized to the original value and n_{ks} ,
- The initial inflow rate, A_{inf} and its declining time scale τ_{inf} ,
- The outflow fraction f_{out} ,

- The IMF slope at the low- and high-mass ends, α_1 and α_2 ,

For more details about model calculations we refer to §3 in Paper I.

3.2 Gas vs stellar metallicity

In Paper I we extensively explore the parameter space to find the parameter combination that allows us to reproduce the observed gas and stellar metallicities of local star forming galaxies simultaneously. Since the gas metallicity is generally higher than the stellar metallicity, especially in low mass galaxies, the parameters that regulate gas and stellar metallicities need to be decoupled, and the metal production at early times needs to be suppressed. Since metal enrichment in the ISM is mainly driven by short-lived Type-II supernovae, the gas metallicity is regulated by very recent evolutionary processes. Stellar metallicity, instead, reflects the whole process of galaxy evolution. Therefore, an effective way of separating the drivers of gas and stellar metallicity is to impose a time dependence on the key processes affecting the metal enrichment.

3.3 Time-dependent metal outflow/IMF slope

In Paper I we find that only two scenarios with either a time-dependent metal outflow fraction or a time-dependent IMF slope are successful in reproducing the observations. We adopt a linear function to characterize the time evolution of the metal outflow fraction and the IMF slope. Figure 2 illustrates the time dependence of the metal outflow fraction (left-hand panel) and the IMF slope (at a star mass $M_{\star} > 0.5 M_{\odot}$, right-hand panel) as a function of galaxy stellar mass, according to the finding of Paper I. In the variable outflow scenario the metal outflow fraction decreases with time with higher initial metal outflow fractions and a stronger evolution in the least massive galaxies. Given the gas metallicity determined by the empirical N2 method, for a relatively massive, Milky Way-like galaxy ($M_{\star} \sim 6 \times 10^{10} M_{\odot}$), the metal outflow fraction is $\sim 65\%$ and barely changes over a Hubble Time. In contrast, for a low mass galaxy like the Small Magellanic Cloud ($M_{\star} \sim 7 \times 10^9 M_{\odot}$), the metal outflow fraction is high at early times (more than 80%) and gradually decreases to $\sim 70\%$ at the current epoch. The evolution of the IMF slope as a function of time and galaxy stellar mass follows a similar pattern (see right-hand panel of Figure 2).

In a nutshell, the former scenario manipulates *metal retention* in low-mass galaxies implying that *most metals are lost* from the galaxy at early times, while the latter manipulates *metal production* in low-mass galaxies implying that *less metals are produced* at early times.

It should be noted that the exact value of the metal outflow fraction depends on the adopted gas metallicity calibration. For example, with a gas metallicity determined through the R23 method (Pilyugin & Thuan 2005), which typically leads to higher values than the empirical N2 method, the required metal outflow fraction is smaller. We refer the reader to Paper I for a detailed discussion of the dependence of the model parameters on the gas metallicity calibration.

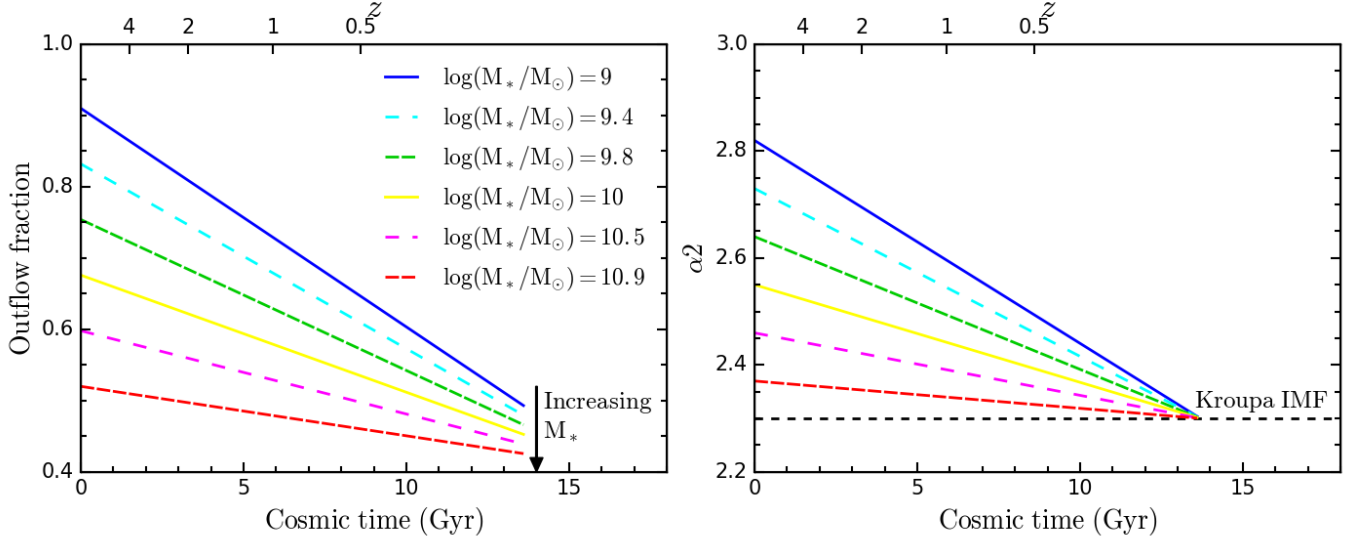


Figure 2. Time evolution of the metal outflow fraction (left-hand panel) and IMF slope at the high-mass end (right-hand panel) as a function of galaxy stellar mass adopted in the variable metal outflow and variable IMF models which will be shown in Figure 3.

3.4 The mass-metallicity relationships

Based on these two scenarios we succeeded at reproducing simultaneously the MZR_{gas} , the MZR_{star} , and the mass-SFR relation of local star-forming galaxies. In an accompanying study (Lian et al. 2018) we extended this model to also include spatial information and modelled the metallicity gradients of local star-forming galaxies observed with SDSS/MaNGA (Goddard et al. 2017). We showed that time-dependent metal outflow fractions or IMF slopes leading to the suppression of early metal enrichment at large radii are required to match gas- and stellar metallicity gradients simultaneously.

In this work we focus on the redshift evolution. The star formation law is assumed not to evolve with redshift. The adopted values for the parameters used in the variable metal outflow and variable IMF model flavours shown in Figure 3 are listed in Table 1. For simplicity we adopt a physical size of 5 kpc for all models independently of redshift. The effect of potential galaxy size evolution on the chemical evolution can be compensated by adopting different gas accretion time scales in order to keep the same gas surface density at any given redshift.

4 RESULTS

We compare the predictions of our models with the MZR_{gas} derived from data at various redshifts ($z \sim 3.5$ to $z \sim 0$) in Figure 3. The models of this work are shown as solid (gas metallicity) and dashed (stellar metallicity) black lines, with thick and thin lines referring to the two model flavours (outflow and IMF model). In order to construct the predicted MZR_{gas} and MZR_{star} (open and filled circles in Figure 3) we calculate models for six different final stellar masses.

Coloured lines and symbols are observational literature results for gas metallicities following the colour scheme and symbol style of Figure 1. The observed mass-stellar metallicity relation of local galaxies from Lian et al. (2018) is

shown as a grey dashed line with the grey area indicating the 1σ scatter of the distribution. Grey triangles, hexagons, and stars in the upper middle panel are the observed stellar metallicities of early-type galaxies at $z \sim 0.7$ (Ziegler et al. 2005; Gallazzi et al. 2014; Comparat et al. 2017; Lonoce et al. 2019). Grey symbols in the upper right panel indicate the median stellar metallicity of samples of early-type galaxies at $z \sim 1.6$ (Onodera et al. 2015; Lonoce et al. 2015; Saracco, Gargiulo, Ciocca & Marchesini 2017) while the hexagons in the bottom middle panel represent the observations of individual galaxies at $z > 3$ from Sommariva et al. (2012).

4.1 Gas metallicity evolution

It can be seen that the predictions of both the variable metal outflow and variable IMF model are nearly identical in this plane of gas metallicity vs stellar mass, and both match the redshift evolution of the MZR_{gas} very well. As these same models also reproduce the local relations (Paper I), they naturally connect the gas metallicities observed in high redshift galaxies with the gas and stellar metallicities measured in galaxies locally.

As already noted, the predictions of the two model flavours (time-dependent metal outflow vs time-dependent IMF slope) are degenerate in the parameter space shown in Figure 3. In other words, both mechanisms could be at work. For a detailed discussion of the pros and cons of these two models we refer to Lian et al. (2018). It is worth noting, though, that the required trend of the IMF as a function of galaxy stellar mass is opposite to the IMF variation argued for local massive quiescent galaxies in order to reproduce their near-IR spectral features (Conroy & van Dokkum 2012; Cappellari et al. 2012; Parikh et al. 2018).

4.2 Gas vs stellar metallicity evolution

Our model also predicts the redshift evolution of MZR_{star} shown as dashed lines in Figure 3. It is interesting to note

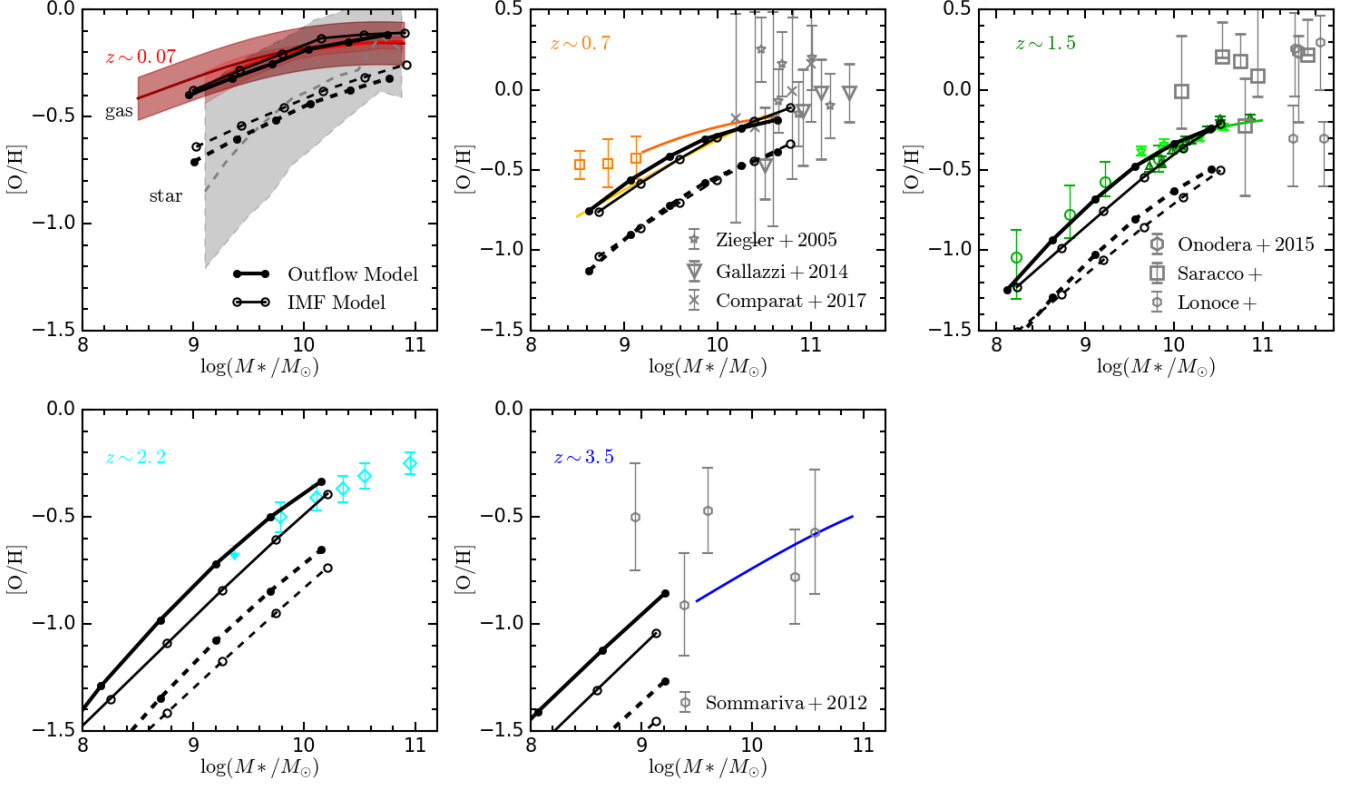


Figure 3. The mass-metallicity relation of star-forming galaxies for various redshift bins (see legend in the panels). Our models are shown as black solid (gas metallicity) and dashed (stellar metallicity) lines, with thick and thin lines referring to two model flavours (outflow and IMF model, see text for more detail). The coloured lines and symbols are observational data of gas metallicities following the colour scheme and symbol style of Figure 1. The observed mass-stellar metallicity relation of local galaxies from Lian et al. (2018) is shown as gray dashed line with the gray area indicating the width of the distribution. Other data for stellar metallicities of galaxies at high redshift are shown as gray symbols (see legend in the panels).

that the MZR_{gas} and MZR_{star} have very different slopes in the local universe, but similar slopes at high redshift with the MZR_{star} being significantly steeper than the MZR_{gas} today. In other words, the MZR_{gas} has experienced a stronger evolution in the shape than the MZR_{star} with the most significant *increase of gas metallicity in low-mass galaxies*. The predicted parallel slope of the MZR_{gas} and MZR_{star} at $z > 1.5$ suggests that the physical drivers of the two relations are linked at early times and decouple at $z \sim 1.5$, i.e. past the epoch of maximum of the cosmic star formation rate.

4.3 Stellar metallicities at high redshifts

There are not many observational constraints on the redshift evolution of the MZR_{star} due to the challenge of obtaining high quality spectra of distant galaxies with a reliable detection of the stellar continuum and absorption features. Existing samples in the literature often focus on passive, early-type galaxies or contain a mix of star-forming and passive galaxies. Ziegler et al. (2005) obtain stellar metallicities for a sample of 13 early-type galaxies between redshift 0.2 and 0.4. They conclude that the stellar metallicities are well consistent with those of the local counterparts. Gallazzi et al. (2014) push to somewhat higher redshifts and larger samples and derive the MZR_{star} for ~ 70 star-forming and passive

galaxies at $z \sim 0.7$ with $M_* > 10^{10} M_\odot$. They conclude that galaxies at ~ 0.7 are systematically more metal poor in their stellar populations than their local counterparts at ~ 0.13 dex. Comparat et al. (2017) derive stellar population properties for a large sample of intermediate redshift galaxies, including star forming emission-line galaxies and luminous red galaxies, from the Extended Baryon Oscillation Spectroscopic Survey, eBOSS (Dawson, et al. 2016; Blanton, et al. 2017; Abolfathi, et al. 2018) using full spectral fitting with FIREFLY. Lonoce et al. (2015, 2019) present individual measurements for a sample of four massive galaxies between redshifts $z \sim 1.4$ and $z \sim 2$, and (Onodera et al. 2015) provides a measurement of stellar metallicity for a stacked spectrum of a sample of galaxies around this same redshift. Metallicity measurements of further six early-type galaxies in this redshift bin are provided by Saracco et al (in prep) selected from their sample presented in Saracco, Gargiulo, Ciocca & Marchesini (2017).

All these studies show that massive galaxies were already metal-rich and dominated by old stellar populations at those early epochs. Finally, Sommariva et al. (2012) derive stellar metallicities for a sample of star-forming galaxies at $z > 3$ based on UV absorption features and found the stellar metallicities in these galaxies to be broadly consistent with the gas phase ones.

The data is shown in Figure 3 as open grey symbols.

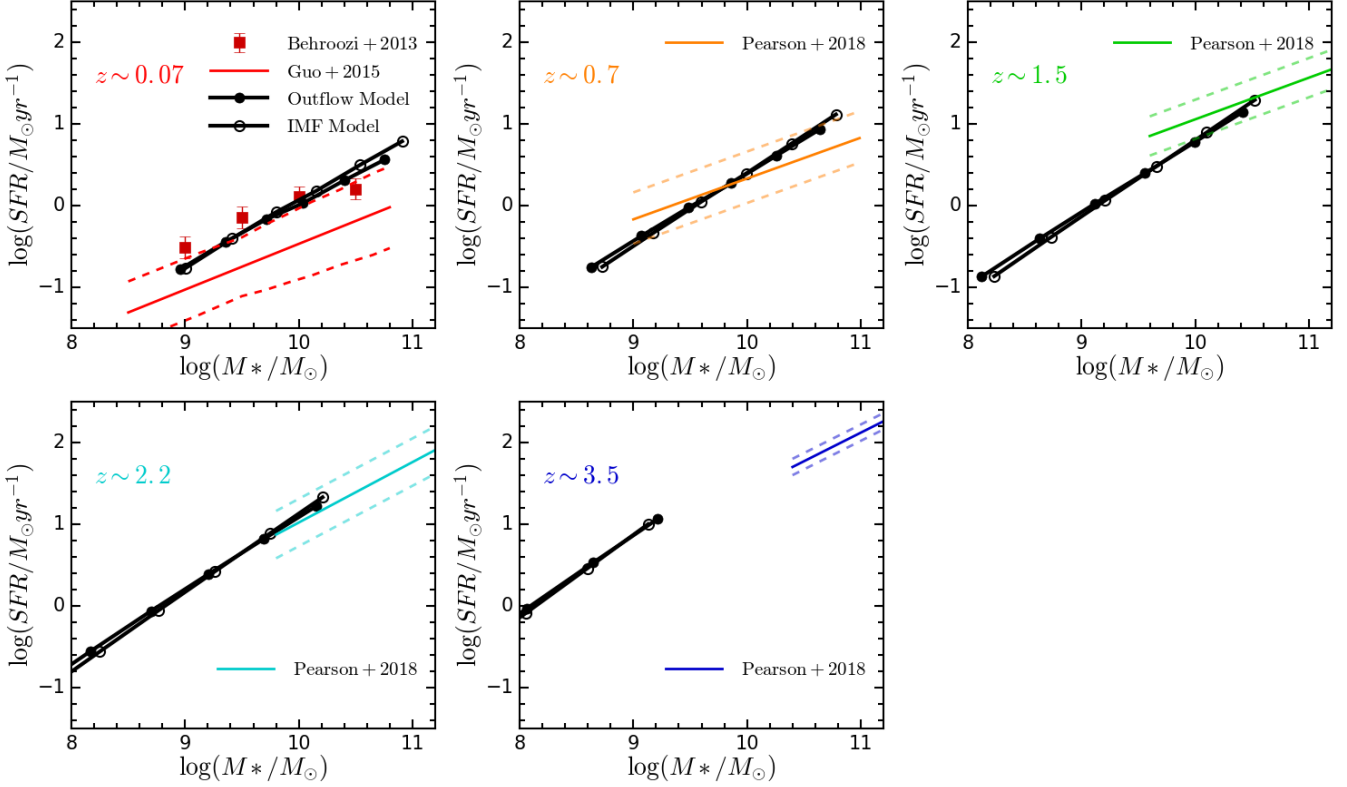


Figure 4. Comparison between the observations and prediction of chemical evolution models in the mass-SFR relation at different redshifts. Each panel indicates one redshift bin with the same colour scheme in Figure 3. Solid black lines connected by filled and empty circles indicate the prediction of models based on time-dependent metal outflow and time-dependent IMF scenario, respectively. The observed local mass-SFR relation are taken from Behroozi et al. (2013); Guo et al. (2015) while mass-SFR relations beyond local universe are taken from Pearson et al. (2018). Dashed lines and error bars show the scatter of the data distribution when applicable.

Most stellar metallicities at high redshift are higher than predicted by our model (dashed lines in extrapolation). This ought to be expected since the observed high- z stellar metallicities refer to quiescent, early-type galaxies, for which the stellar metallicity is generally higher than in star-forming galaxies (Peng et al. 2015). The only exception is the lowest-stellar mass data point by Gallazzi et al. (2014) at $z \sim 0.7$, which is likely the only one dominated by star-forming galaxies. The Gallazzi et al. results imply significantly lower metallicities in the stars than in the gas also in galaxies at redshift $z \sim 0.7$ in good agreement with the prediction from our model.

Some of the measurements in Sommariva et al. (2012) are higher than the prediction of our model at $z > 3$ which may be due to the different stellar populations represented by the data and the model. Sommariva et al. (2012) use UV absorption features to derive the stellar metallicity, which gives more weight to the properties of the youngest, most metal-rich stars. The mass-weighted stellar metallicity predicted by our model, instead, represents the average value over all ages of the stellar population.

4.4 The mass-SFR relationship

We further examine our model by comparing the predicted mass-SFR relationship (i.e. main sequence, Elbaz et al. 2007;

Noeske et al. 2007; Renzini & Peng 2015) with observations at the various redshift intervals. The result is shown in Figure 4. Each panel indicates one redshift bin with the same colour scheme as in Figure 3. Also the symbols and line styles are the same as in Figure 3. The observed local mass-SFR relation is adopted from Guo et al. (2015) based on $H\alpha$ in combination with $22\mu\text{m}$ observations from WISE and Behroozi et al. (2013) with SFRs adopted from Salim et al. (2007) and Robotham & Driver (2011) based on UV observations with *GALEX*. The mass-SFR relations beyond the local universe are taken from a recent work by Pearson et al. (2018) based on deep Herschel far-IR observations. Dashed lines and error bars indicate the 1σ scatter of the data distribution. The local SFR measurements are broadly consistent within the 1σ scatter. The difference may be due to the difference in sample selection of star-forming galaxies and usage of different SFR indicators which trace the SFR over different time scales. The SFR measured by mid-IR observations in the local universe should in principle be consistent with the SFR based on far-IR observations at high redshift given the good correlation between mid- and far-IR luminosity with the total IR luminosity of star-forming galaxies (e.g. Rieke et al. 2009).

It can be seen that the mass-SFR relations at different redshifts predicted by our chemical evolution model are in generally good agreement with the observations. The predicted slope is slightly flatter than the one observed at inter-

mediate redshifts, but still consistent within the 1σ error. A further adjustment of the model parameters controlling the star formation efficiency and the inflow/outflow rates can mitigate the discrepancy, which, however, goes beyond the scope of this paper.

5 DISCUSSION

As shown in Figure 3 the MZR_{gas} has been flattening with time since $z \sim 1.5$. Massive star-forming galaxies reach their final gas metallicity already at that redshift, while the gas metallicity in low-mass galaxies kept increasing steadily until today. This chemical downsizing pattern (Maiolino et al. 2008) imprinted in the metal-enrichment histories of star-forming galaxies is similar, but not the same as the downsizing seen in the stellar population properties of passive galaxies (e.g., Cowie et al. 1996; Heavens et al. 2004; Thomas et al. 2005, 2010). The latter is attributed to quenching and caused by the fact that more massive galaxies quench earlier. The chemical downsizing discussed here, instead, is detected in a population of galaxies forming stars throughout, and must therefore be attributed to the process of metal enrichment itself.

5.1 The origin of the mass-metallicity relation

The redshift evolution of the MZR_{gas} requires two separate mechanisms to be at play. The metal enrichment 1) needs to be suppressed at early times in low-mass galaxies, and 2) must come to a halt in massive galaxies at an epoch around $z \sim 1.5$. A time-dependent mechanism that regulates metal enrichment in galaxies is required. One possibility is to invoke a time-dependence in the star formation efficiency (SFE), predominantly in lower-mass galaxies, such that the SFE increases with cosmic time. Based on an analytical galaxy evolution model, Lilly et al. (2013) investigate the cosmic evolution of the MZR_{gas} and show that a decline in SFE with time can drive the evolution of the MZR_{gas} . Sakstein et al. (2011) come to a similar conclusion based on a semi-analytical model showing that the same parameters that regulate the SFR are also responsible for the evolution of MZR_{gas} . However, as discussed in Paper I, this time-dependent SFE scenario fails at reproducing simultaneously the MZR_{gas} and MZR_{star} in the local universe. In such a model the predicted MZR_{star} evolves in parallel to the MZR_{gas} leading to an MZR_{star} that is too shallow compared to observations, as shown in Figure 3 and discussed in Paper I.

5.2 Time-dependent metal outflow vs IMF slope

With the present study we present a model that matches both, the local mass-metallicity relation of stars and gas, as well as the redshift evolution of the MZR_{gas} . This model is based on a time-dependent metal outflow loading factor or a time-dependent IMF slope rather than a time-dependent star formation efficiency. In both these model flavours, the production of metals is substantially suppressed in low-mass galaxies at early times, which explains both the low stellar metallicity in today's low-mass galaxies and the low gas metallicity in high-redshift low-mass galaxies.

It is plausible to assume that a shallower gravitational well at earlier times leads to a higher metal loading factor in galactic winds. This naturally leads to a dependence on cosmic time, galaxy mass, and galaxy radius as inferred in our model. We note that such mass dependence of the metal loading factor is also required by the chemical evolution model by Peeples & Shankar (2011) to explain the observed correlation of gas metallicity and gas fraction with galaxy mass. The time-dependent IMF scenario, instead, could be caused by a metallicity dependence of the IMF if steeper IMFs are generated in lower metallicity environments. This is not implausible, but clear observational evidence for such a behaviour is currently missing (Bastian et al. 2010; Bate 2014) and opposite trends seem to exist in simulations (Kroupa et al. 2013; Chabrier et al. 2014).

To summarise, the redshift evolution of the MZR_{gas} is driven by a combination of mass-dependent star formation efficiency and a time-dependent suppression of metal enrichment in low-mass galaxies through either efficient metal outflow or a steeper IMF slope at early times.

5.3 Gas metallicities in massive galaxies

It is interesting to note that the gas metallicity in massive star-forming galaxies stops increasing with cosmic time at around $z \sim 1.5$ despite ongoing star formation activity. This saturation in the metal enrichment is predicted naturally by any chemical evolution model. The reason is that the metal enrichment in the gas is the result of competing effects between star formation-driven metal production and dilution caused by accretion of pristine gas. In the low metallicity regime, the dilution effect is inefficient compared to the star formation-driven metal production. Once the gas metallicity becomes high enough, the dilution effect due to gas accretion becomes efficient. Therefore, saturation occurs when the gas metallicity reaches a high enough value for the dilution effect to balance the metal production. At this point the metallicity settles at the effective yield of metal production (Edmunds 1990; Thomas, Greggio & Bender 1999). It is interesting to note that the saturation time for massive star forming galaxies ($M_* > 10^{10.5} M_\odot$) is very close to the peak of the cosmic star formation history ($z \sim 2$, Madau & Dickinson 2014).

This saturation feature is also evident in Figure 12 in Paper I where we explore all possible cosmic evolution of gas and stellar metallicity under various model parameter configuration, and is a natural explanation for the change of evolution mode of the MZR_{gas} at $z \sim 1.5$ (Lian et al. 2015). At redshift $z > 1.5$, the gas metallicity is still far from the threshold value and metal enrichment is still efficient also in massive galaxies. As a consequence only the zero-point, but not the slope of the MZR_{gas} evolves from $z \sim 3.5$ to $z \sim 1.5$. Since more massive galaxies generally have higher gas mass surface density and therefore higher efficiency in converting gas into stars and metal production, they reach the saturated metallicity earlier than less massive galaxies. At $z \sim 1.5$, the gas metallicity in massive galaxies ($M_* > 10^{10.5} M_\odot$) has first reached the threshold value and saturates. As a result, the high mass end of MZR_{gas} remains unchanged after $z \sim 1.5$ and the MZR_{gas} becomes flatter with time. It should be noted that the stellar mass of a galaxy is increasing along with the metal enrichment

Table 1. Parameter ranges of the time dependent chemical enrichment models (for a variable outflow and a variable IMF) shown in Figure 4.

	A_{ks}	$A_{\text{ks,i}}$	n_{ks}	A_{inf} $\text{M}_{\odot}\text{yr}^{-1}$	τ_{inf} Gyr	f_{out}	$f_{\text{out,i}}$	α_1	α_2	α_2
Variable outflow	1	0.63	1.5	[0.20,19.95]	[40,6.6]	[0.50,0.43]	[0.92,0.50]	1.3	2.3	2.3
Variable IMF	1	[1,0.50]	1.5	[0.20,25.12]	[40,6.6]	[0.40,0.35]	[0.40,0.34]	1.3	[2.85,2.3]	2.3

process. Therefore, the evolution in the mass-gas metallicity relation indicates that the metal enrichment of galaxies progresses at a faster pace than their mass assembly until they reach the threshold metallicity of saturation. Since the saturation value of the gas metallicity depends on the IMF, the invariant gas metallicity of the massive galaxies ($M_* > 10^{10.5} \text{ M}_{\odot}$) from $z \sim 1.5$ to $z \sim 0$ serves as a strong evidence for an invariant IMF in those galaxies in this redshift range.

5.4 Cosmological models

Based on semi-analytical models and cosmological hydrodynamical simulations, Guo et al. (2016) found the cosmic evolution of the MZR_{gas} to be inconsistent between these two theoretical approaches. A flattening of the MZR_{gas} and with increasing gas metallicity over cosmic time is predicted by the hydrodynamical simulations, which is more consistent with the observations and the chemical evolution model presented here. The lack of evolution predicted by the semi-analytical models may be due to a deficient treatment of gas flows (Guo et al. 2016).

A similar trend of a flattening of the MZR_{gas} with cosmic time is also found by Taylor & Kobayashi (2016) based on their cosmological hydrodynamical simulations. Interestingly, their simulation further shows that the MZR_{star} mainly evolves in zero point and not slope in contrast to the MZR_{gas} . This prediction by the model is in good qualitative agreement with the prediction of our numerical chemical evolution model. Although the state-of-art cosmological hydrodynamical simulations seem to predict a cosmic evolution trend of MZR_{gas} broadly consistent with observations, it should be pointed out that they still face difficulties to match the exact shape of the observed MZR_{gas} at different redshifts (see Figure 12 in Guo et al. 2016 and Figure 8 in Taylor & Kobayashi 2016).

6 CONCLUSIONS

We study the origin and cosmic evolution of the mass-metallicity relation (MZR) in star-forming galaxies based on a full, numerical chemical evolution model which was designed to match the local MZRs for both gas and stars simultaneously (Lian et al. 2018, Paper I).

Our model accounts for three basic physical processes that regulate the chemical evolution of galaxies, namely gas inflow, gas outflow, and star formation. The main characteristic of this model is that a time-dependent metal enrichment process is invoked assuming either a time-dependent metal outflow with higher metal loading factors in galactic winds at early times, or a time-dependent IMF with steeper IMF

slopes at early times. The former regulates the *metal retention* in galaxies so that more metals are lost at early times, while the latter regulates the *metal production* so that less metals are produced at early times. The aim of the present paper is to test the predictions by these models for the redshift evolution of the MZR_{gas} and compare them with observational data at various redshifts up to $z \sim 3.5$.

To this end we analyse our own sample drawn from SDSS and discussed in Paper I and adopt further data sets from the literature covering the redshift range $0 \leq z \leq 3.5$. We homogenise the sample by correcting stellar masses to the stellar mass based on the Kroupa IMF (Kroupa 2001), and gas metallicities to the empirical N2 method (Pettini & Pagel 2004). The data suggest a two-phase evolution with a transition point around $z \sim 1.5$. Before that epoch the MZR_{gas} has been evolving parallel with no evolution in the slope. After $z \sim 1.5$ the MZR_{gas} started flattening until today. Hence the gas metallicity of the most massive star forming galaxies has not been evolving since that epoch. This is an epoch just past the peak of the cosmic star formation rate (Madau & Dickinson 2014). Instead, significant evolution has been occurring in the lowest mass galaxies until today.

This is in good agreement with the steep MZR_{star} of local star-forming galaxies, which indeed implies a steep MZR_{gas} at early times. This delayed-enrichment model matches the redshift evolution of the MZR_{gas} very well. Hence we have a working model which naturally connects the gas metallicities observed in high redshift galaxies with the gas and stellar metallicities measured in galaxies locally. Our model also reproduces the evolution of the main sequence, hence the correlation between galaxy mass and star formation rate.

We further discuss the main drivers of the mass-metallicity relation and its evolution with redshift. It turns out that the redshift evolution of the MZR_{gas} requires two separate mechanisms to be at play. The metal production needs to be suppressed at early times in low-mass galaxies, and must come to a halt in massive galaxies at an epoch around $z \sim 1.5$. Our model invoking a time-dependent mechanism that regulates star formation in galaxies through either a time-dependent metal outflow or a time-dependent IMF slope matches this behaviour very well.

Our model also predicts the redshift evolution of the MZR_{star} . There are not many observational constraints on the redshift evolution of the MZR_{star} due to the challenges in the observations. We compare the prediction of our model with data from the literature. The latter mostly contains data of massive, quenched early-type galaxies, while here we model the evolution of star-forming galaxies. As a consequence most of the stellar metallicities at high redshifts are higher in the data than predicted by our model as expected.

Data of stellar metallicities of lower-mass ($< 10^{11} M_{\odot}$), star-forming galaxies at high redshift is needed for a meaningful test of our model.

ACKNOWLEDGEMENTS

The Science, Technology and Facilities Council is acknowledged for support through the Consolidated Grant Cosmology and Astrophysics at Portsmouth, ST/N000668/1. This work is also supported by the National Natural Science Foundation of China (no. 11673004). Numerical computations were done on the Sciama High Performance Compute (HPC) cluster which is supported by the ICG, SEPnet and the University of Portsmouth.

REFERENCES

- Alam, S., Albareti, F. D., Allende Prieto, C., et al. 2015, *ApJS*, 219, 12
- Abolfathi B., et al., 2018, *ApJS*, 235, 42
- Andrews, B. H., & Martini, P. 2013, *ApJ*, 765, 140
- Baldwin, J. A., Phillips, M. M., & Terlevich, R. 1981, *PASP*, 93, 5
- Blanton M. R., et al., 2017, *AJ*, 154, 28
- Bastian, N., Covey, K. R., & Meyer, M. R. 2010, *ARA&A*, 48, 339
- Bate, M. R. 2014, *MNRAS*, 442, 285
- Behroozi, P. S., Wechsler, R. H., & Conroy, C. 2013, *ApJ*, 770, 57
- Bolzonella M., et al., 2010, *A&A*, 524, A76
- Brooks, A. M., Governato, F., Booth, C. M., et al. 2007, *ApJL*, 655, L17
- Calura, F., Pipino, A., Chiappini, C., Matteucci, F., & Maiolino, R. 2009, *A&A*, 504, 373
- Cappellari, M., McDermid, R. M., Alatalo, K., et al. 2012, *Nature*, 484, 485
- Cardelli, J. A., Clayton, G. C., & Mathis, J. S. 1989, *ApJ*, 345, 24
- Chabrier, G., Hennebelle, P., & Charlot, S. 2014, *APJ*, 796, 75
- Comparat, J., Maraston, C., Goddard, D., et al. 2017, *arXiv:1711.06575*
- Conroy, C., & van Dokkum, P. G. 2012, *ApJ*, 760, 71
- Cowie, L. L., Songaila, A., Hu, E. M., & Cohen, J. G. 1996, *AJ*, 112, 839
- Dawson K. S., et al., 2016, *AJ*, 151, 44
- Edmunds M. G., 1990, *MNRAS*, 246, 678
- Elbaz, D., Daddi, E., Le Borgne, D., et al. 2007, *A&A*, 468, 33
- Erb, D. K., Steidel, C. C., Shapley, A. E., Pettini M., Reddy N. A., Adelberger K. L., 2006, *ApJ*, 646, 107
- Gallazzi, A., Charlot, S., Brinchmann, J., White, S. D. M., & Tremonti, C. A. 2005, *MNRAS*, 362, 41
- Gallazzi, A., Bell, E. F., Zibetti, S., Brinchmann, J., & Kelson, D. D. 2014, *ApJ*, 788, 72
- González Delgado, R. M., Cid Fernandes, R., García-Benito, R., et al. 2014, *ApJL*, 791, L16
- Guo, K., Zheng, X. Z., Wang, T., & Fu, H. 2015, *ApJL*, 808, L49
- Guo, Q., Gonzalez-Perez, V., Guo, Q., et al. 2016, *MNRAS*, 461, 3457
- Heavens, A., Panter, B., Jimenez, R., & Dunlop, J. 2004, *Nature*, 428, 625
- Henry, A., Martin, C. L., Finlator, K., & Dressler, A. 2013, *ApJ*, 769, 148
- Henry, A., Scarlata, C., Domínguez, A., et al. 2013, *ApJL*, 776, L27
- Johansson, J., Thomas, D., & Maraston, C. 2012, *MNRAS*, 421, 1908
- Kashino, D., More, S., Silverman, J. D., et al. 2017, *ApJ*, 843, 138
- Kennicutt, R. C., Jr. 1998, *ARA&A*, 36, 189
- Kewley, L. J., Dopita, M. A., Sutherland, R. S., Heisler, C. A., & Trevena, J. 2001, *ApJ*, 556, 121
- Kewley, L. J., & Ellison, S. L. 2008, *ApJ*, 681, 1183
- Köppen, J., Weidner, C., & Kroupa, P. 2007, *MNRAS*, 375, 673
- Kroupa, P. 2001, *MNRAS*, 322, 231
- Kroupa, P., Weidner, C., Pflamm-Altenburg, J., et al. 2013, *Planets, Stars and Stellar Systems. Volume 5: Galactic Structure and Stellar Populations*, 5, 115
- Larson, R. B. 1974, *MNRAS*, 169, 229
- Lequeux, J., Peimbert, M., Rayo, J. F., Serrano, A., & Torres-Peimbert, S. 1979, *A&A*, 80, 155
- Lian, J. H., Li, J. R., Yan, W., & Kong, X. 2015, *MNRAS*, 446, 1449
- Lian, J., Hu, N., Fang, G., Ye, C., & Kong, X. 2016, *ApJ*, 819, 73
- Lian, J., Thomas, D., Maraston, C., et al. 2018, *MNRAS*, 474, 1143
- Lilly, S. J., Carollo, C. M., Pipino, A., Renzini, A., & Peng, Y. 2013, *ApJ*, 772, 119
- Lonoce I., et al., 2015, *MNRAS*, 454, 3912
- Lonoce I., et al., 2019, *MNRAS*, in preparation
- Ly, C., Malkan, M. A., Rigby, J. R., & Nagao, T. 2016, *ApJ*, 828, 67
- Madau, P., & Dickinson, M. 2014, *ARA&A*, 52, 415
- Maiolino, R., Nagao, T., Grazian, A., et al. 2008, *A&A*, 488, 463
- Mannucci, F., Cresci, G., Maiolino, R., Marconi, A., & Gnerucci, A. 2010, *MNRAS*, 408, 2115
- Maraston, C., & Strömbäck, G. 2011, *MNRAS*, 418, 2785
- Noeske, K. G., Weiner, B. J., Faber, S. M., et al. 2007, *ApJL*, 660, L43
- Onodera, M., Carollo, C. M., Renzini, A., et al. 2015, *ApJ*, 808, 161
- Panther, B., Jimenez, R., Heavens, A. F., & Charlot, S. 2008, *MNRAS*, 391, 1117
- Parikh, T., Thomas, D., Maraston, C., et al. 2018, *MNRAS*, 478, 1000
- Pearson, W. J., Wang, L., Hurley, P. D., et al. 2018, *arXiv:1804.03482*
- Peeples, M. S., & Shankar, F. 2011, *MNRAS*, 417, 2962
- Peng, Y., Maiolino, R., & Cochrane, R. 2015, *Nature*, 521, 192
- Pettini, M., & Pagel, B. E. J. 2004, *MNRAS*, 348, L59
- Pilyugin, L. S., & Thuan, T. X. 2005, *ApJ*, 631, 231
- Pforr J., Maraston C., Tonini C., 2012, *MNRAS*, 422, 3285
- Renzini, A., & Peng, Y.-j. 2015, *ApJL*, 801, L29
- Rieke, G. H., Alonso-Herrero, A., Weiner, B. J., et al. 2009, *ApJ*, 692, 556
- Robotham, A. S. G., & Driver, S. P. 2011, *MNRAS*, 413, 1000

- 2570
- Sakstein, J., Pipino, A., Devriendt, J. E. G., & Maiolino, R. 2011, MNRAS, 410, 2203
- Salim, S., Rich, R. M., Charlot, S., et al. 2007, ApJS, 173, 267
- Saracco P., Gargiulo A., Ciocca F., Marchesini D., 2017, A&A, 597, A122
- Savaglio, S., Glazebrook, K., Le Borgne, D., et al. 2005, ApJ, 635, 260
- Sommariva, V., Mannucci, F., Cresci, G., et al. 2012, A&A, 539, A136
- Spergel, D. N., Verde, L., Peiris, H. V., et al. 2003, ApJS, 148, 175
- Taylor, P., & Kobayashi, C. 2016, MNRAS, 463, 2465
- Thomas, D., Maraston, C., Bender, R., & Mendes de Oliveira, C. 2005, ApJ, 621, 673
- Thomas D., Greggio L., Bender R., 1999, MNRAS, 302, 537
- Thomas, D., Maraston, C., Schawinski, K., Sarzi, M., & Silk, J. 2010, MNRAS, 404, 1775
- Tissera, P. B., De Rossi, M. E., & Scannapieco, C. 2005, MNRAS, 364, L38
- Tremonti, C. A., Heckman, T. M., Kauffmann, G., et al. 2004, ApJ, 613, 898
- Veilleux, S., Cecil, G., & Bland-Hawthorn, J. 2005, ARA&A, 43, 769
- Wilkinson, D. M., Maraston, C., Thomas, D., et al. 2015, MNRAS, 449, 328
- Wilkinson, D. M., Maraston, C., Thomas, D., et al. 2017, MNRAS, submitted
- Worthey G., 1994, ApJS, 95, 107
- Yabe, K., Ohta, K., Iwamuro, F., et al. 2014, MNRAS, 437, 3647
- Zahid, H. J., Kewley, L. J., & Bresolin, F. 2011, ApJ, 730, 137
- Zahid, H. J., Kashino, D., Silverman, J. D., et al. 2014, ApJ, 792, 75
- Ziegler B. L., Thomas D., Böhm A., Bender R., Fritz A., Maraston C., 2005, A&A, 433, 519